01 Jul 2023

Detection Of Critical Cancer Cells In Human Organs Using Dual Demodulation Photonic Crystal Fiber: Numerical Study

Farhan Mumtaz
Missouri University of Science and Technology, mfmawan@mst.edu

Recommended Citation

F. Mumtaz, "Detection Of Critical Cancer Cells In Human Organs Using Dual Demodulation Photonic Crystal Fiber: Numerical Study," *Results in Optics*, vol. 12, article no. 100493, Elsevier, Jul 2023.
The definitive version is available at https://doi.org/10.1016/j.rio.2023.100493

Results in Optics 12 (2023) 100493

Contents lists available at ScienceDirect

Results in Optics

journal homepage: www.sciencedirect.com/journal/results-in-optics

Detection of critical cancer cells in human organs using dual demodulation photonic crystal fiber: Numerical study

Farhan Mumtaz

Department of Electrical and Computer Engineering, Missouri University of Science and Technology, Rolla, MO 65409-0040, USA

ARTICLE INFO

Keywords:
Photonic crystal fiber
Malignant cancerous cells
Optical sensor
Dual demodulation approach

ABSTRACT

This study reports a novel approach for early detection of malignant cancer cells in human organs using a birefringent photonic crystal fiber (PCF)-based optical sensor with dual demodulation. The PCF injects light into the middle hole, enhancing the radiated evanescent field. Analytes injected through the core cause a wavelength shift, measured by peak or dip shift. The proposed sensor has an optimal sensitivity of −7,940 nm/RIU, −8,265 nm/RIU, −9,747 nm/RIU, −9,006 nm/RIU, and −8,994 nm/RIU by peak shift and −8,745 nm/RIU, −10,728 nm/RIU, −8,721 nm/RIU, −10,113 nm/RIU, and −11,150 nm/RIU by dip shift for CRT-(Cervical tissue), BLD-(Blood), ADG-(Adrenal gland), BRT-(Breast) type-1 and type-2 cells, respectively. The PCF sensor presents a shorter sensing length of 550 μm. Results suggest the sensor is effective in detecting malignant neoplastic cells in earlier stages, making it a promising tool for cancer diagnosis and treatment.

1. Introduction

The incidence of cancer has been on the rise in recent years, making it a significant public health concern (Jamil and Khan, 2020). Cancer is a genetic condition that can result from inherited genetic mutations (Yoshikawa et al., 2020), chronic infections (Samaras et al., 2010), exposure to carcinogens (Hecht, 2003), an unhealthy diet and lifestyle (Ali et al., 2011), toxic chemicals (Taya et al., 2022), and environmental toxins (Saha et al., 2020). The uncontrolled and unchecked cell growth associated with cancer can lead to the development of malignant tumors and the spread of cancer throughout the body, resulting in mortality. Early detection and treatment of cancer are crucial for improving patient outcomes and reducing mortality rates. Various methods are available for cancer detection, including imaging techniques, biopsy, and blood tests. However, the development of novel approaches, such as the use of optical sensors and photonic crystal fibers, holds great promise for the early identification of cancer cells in different human organs. The use of these approaches can enhance the sensitivity and specificity of cancer detection and contribute to the development of effective treatment strategies for cancer patients.

Fiber-optic sensors have emerged as a promising option for cancer detection, as they can overcome existing obstacles (Singh et al., 2020), and for the diagnosis, several fiber-optic sensors have been reported (Sun et al., 2017; Schartner et al., 2016; Kaur et al., 2022; Bekmurzayeva et al., 2021; Loyez et al., 2019). These sensors include cancer biomarkers detection without labels, sampling malignant human tissue, diagnosing colorectal cancer, detecting picomolar levels of CD44 protein, and identifying brain tumors. Researchers outcome that fiber optic sensors can measure the quantity and stage of malignant cells by monitoring shifts in the refractive index (RI) of cancerous analytes, which indicate RI differences (Azzouz et al., 2022). Photonic crystal fiber (PCF) sensors are microstructured optical fibers that work through total internal reflection theory and photonic band-gap transmission of light. They have shown exceptional performances in the development of biosensing applications over the past three decades due to their high sensitivity, quick procedures, and affordable manufacturing (Anders et al., 2003). By controlling the distribution of air-hole spacing, size, and geometry, PCFs allow for the desired configuration of the effective core (Biswas et al., 2018). In optical sensing, the waveguiding and optical properties of a PCF are improved collectively (Mumtaz et al., 2023).

Numerous studies have been explored by using PCF sensors for detecting various types of cancerous cells. For instance, Eid et al. (Eid et al., 2021) reported a PCF-based biosensor with a mono-rectangular core to identify skin and blood cancer cells. Abdullah et al. (Bulbul et al., 2020) reported a PCF-based biosensor for detecting breast cancer cells that utilized the Terahertz (THz) regime for computational analysis. Abdel et al. (Abdelghaffar et al., 2022) reported a plasmonic PCF sensing structure that used Zirconium Nitride as a plasmonic material to detect breast cancer cells type-1 with an optimum sensitivity of ~5,700 nm/RIU. Yasli et al. (Yasli, 2021) reported a blended-shaped plasmonic

E-mail address: mfmawan@mst.edu.

https://doi.org/10.1016/j.rio.2023.100493
Received 15 May 2023; Received in revised form 1 July 2023; Accepted 20 July 2023
Available online 24 July 2023

PCF structure for detecting malignant skin, BRT type-1, BRT type-2, ADG, BLD, and CRT cells with maximum sensitivity of 7,142 nm/RIU for the analyte RI of a BRT cancer cell. Mollah et al. (Mollah et al., 2020) reported on a numerical research study on cancerous cells detection and utilized a highly sensitive Sagnac interferometer-based PCF-RI sensor (Sasi et al., 2021), such as BRT type-1, BRT type-2, BLD, and ADG. Jabin et al. (Jabin et al., 2019) also developed a Titanium-coated D-shaped plasmonic-based PCF sensor for detection of malignant cancer cells in various region of human body. Mishra et al. (Mishra et al., 2020) reported computational analysis of a heart-shaped dual-core PCF sensor and achieved the highest sensitivity of 10,000 nm/RIU for BRT cells. These studies demonstrate the significant potential of PCF-based sensors in biosensing applications for cancerous cells due to their customizable optical properties such as, high sensitivity, simple construction, and rapid result processing. Parvin et al. (Parvin et al., 2021) conducted a numerical study on a spectroscopic optical sensor for detecting cancerous cells in various parts of the body, including the cervix, adrenal gland, breast, skin, and blood. Based on their findings, they reported a maximum sensitivity of 95.5% for BRT type-2 cells. Mollah et al. (Mollah et al., 2020) proposed a twin core-PCF for detecting blood cancer by observing spectrum shift using FEM in transmission spectra, and obtained maximum sensitivity of 8571.43 nm/RIU. Ramola et al. (Ramola et al., 2021) proposed a PCF-based SPR biosensor for early cancer detection using numerical FEM analysis. The sensor achieved high sensitivity and FOM using TM and TE modes, with MCF-7 cells, but the sensor's smaller core cross-section may be a limiting factor.

A novel dual demodulation approach is proposed through an optimal design of PCF-based fiber-optic sensors for the detection of various malignant cancer cells in humans. This approach capitalizes on the potential of PCF-based sensors and modifies the optical path through variations in the effective refractive index (RI) of the PCF-sensor as it interacts with different bio-analytes. To determine the RIs of these bio-analytes, normal cells concentrations (30−70%) and cancerous cells concentrations (80%) in liquid form are used. The PCF sensor's micro-structured air-hole formation is adjusted to achieve a sensing length of 550 μm. The COMSOL Multi-physics 6.0® is used to perform model simulations, an average optimal sensitivity of −9,293 nm/RIU by peak tracking and −8708 nm/RIU by dip tracking is achieved for all targeted cancerous cells within a RI range of 1.368 to 1.401, facilitating the differentiation between healthy and carcinogenic cell analytes. These findings highlight the potential of PCF-based sensors in detecting crucial malignant cancer cells in humans.

2. Sensor geometry and operating principle

Fig. 1(a) illustrates the transverse cross-section of the proposed PCF sensor, which includes a central hole and air holes in the cladding region with diameters of $d_a = 1.5$ μm and $d_c = 1.9$ μm, respectively. The pitch, denoted by the symbol $\Lambda = 2.0$ μm, represents the distance between air holes. The central air hole is designed to inject cancerous cell analytes. Fig. 2(b) presents the prespective view of PCF sensor. Table 1 presents the RI values of fluid analytes for malignant and normal cells, with concentrations of 80% and 30% to 70%, respectively. The hosting medium for the cladding region is fused silica, approximated using the Sellmeier equation (Mumtaz et al., 2022; Mumtaz et al., 2022), while the RI for the cladding air holes is assumed to be 1.

$$n_{silica} = \sqrt{1 + \frac{0.6961663\lambda^2}{\lambda^2 - 0.0684043^2} + \frac{0.4079426\lambda^2}{\lambda^2 - 0.1162414^2} + \frac{0.8974794\lambda^2}{\lambda^2 - 9.896161^2}} \quad (1)$$

where λ symbolizes the central operating wavelength. The FEM layout consists of 52 domains, 200 edges, and 196 points, and the mesh comprises 14,984 elements with an average quality of 0.8037 and minimum quality of 0.3646, as depicted in Fig. 1(c). The Perfect Match Layer (PML) is employed as a boundary condition in the simulation to absorb radiation and prevent reflections from the sensor's core area. By effectively absorbing electromagnetic waves at the boundary, the PML ensures that they do not bounce back into the computational region, resulting in a more realistic simulation. This boundary condition reduces unwanted reflections, improving the accuracy of the results and allowing for a reliable analysis of the sensor's behavior.The dual-core region around the central infiltrated hole employs the index-guiding method to confine the injected light by creating a high RI zone. The resulting propagating modes are referred to as super-modes, which are further categorized into four distinct topologies: Even and odd x-pol (polarized) coupled modes, as well as even and odd y-pol coupled modes. The electric (E)-field distributions of the fundamental modes for x-pol and y-pol orientations, corresponding to even and odd modes, are obtained at the central operating wavelength of 1.55 μm. As illustrated in Fig. 2(a-d), the effective RIs of these modes are 1.3995 (y-pol ~ even mode), 1.3967 (y-pol ~ odd mode), 1.3979 (x-pol ~ even mode), and 1.3955 (x-pol ~ odd mode).

Fig. 3 depicts a possible experimental setup for detecting various malignant cancerous analytes (Mumtaz et al., 2020). The input light is introduced to the sensor via a single-mode fiber (SMF) lead-in from a broadband source (BBS) with a flat bandwidth range of 1.4 μm to 2.0 μm. An optical spectrum analyzer (OSA) is used to analyze the injected light as it traverses the sensor and exits through the SMF lead-out on the output side. The interference dip or peak shift in the spectral wavelength domain, which corresponds to the RIs of normal and cancerous cells, is calculated based on the transmission spectra obtained by the OSA (Mumtaz et al., 2023).

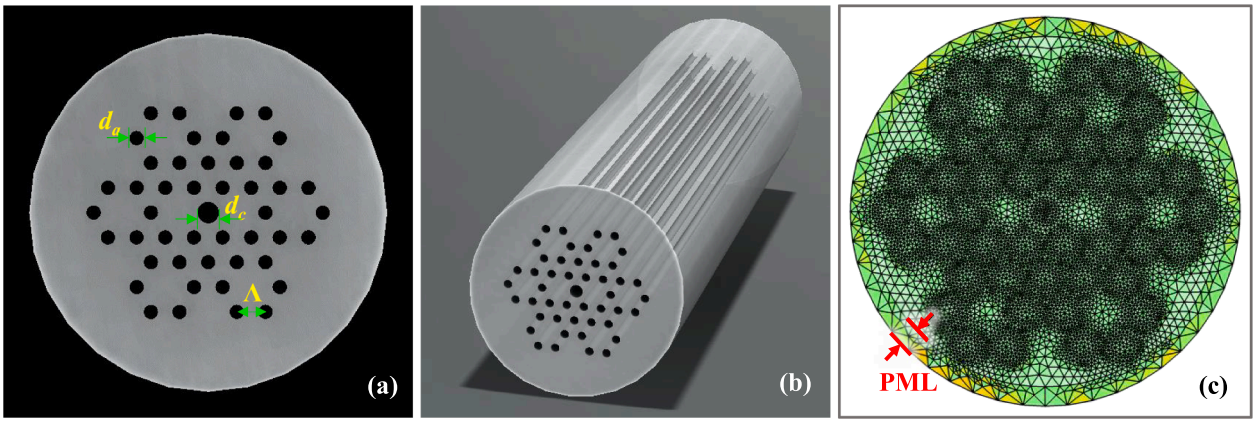

Fig. 1. Proposed PCF sensor: (a) transverse cross-section, (b) longitudinal perspective view, and (c) mesh profile.

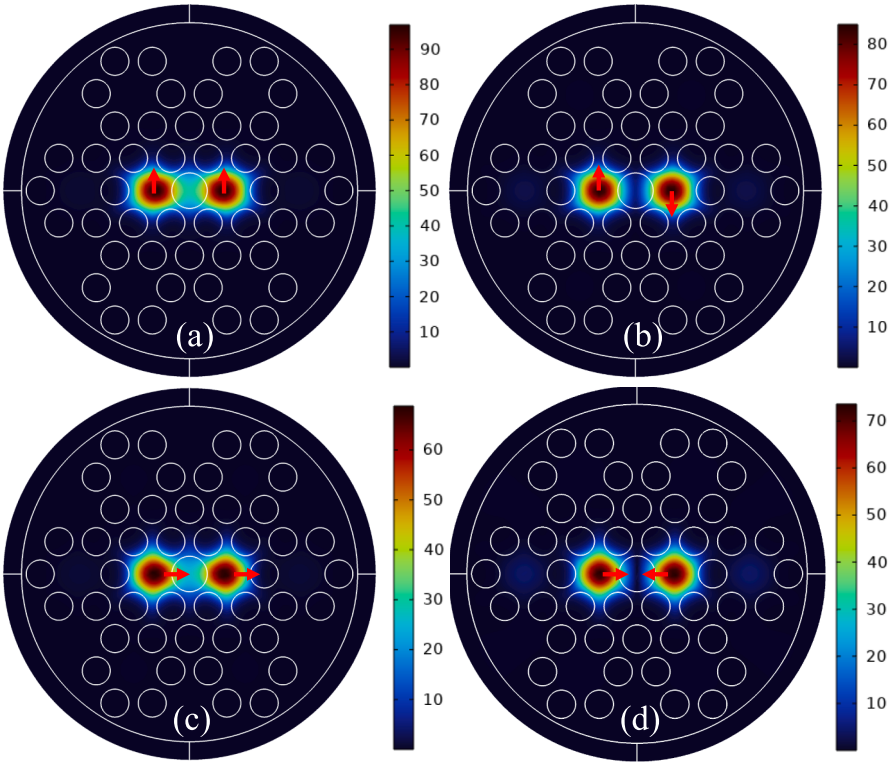

Fig. 2. At the central operating wavelength of 1.55 m, the E-field distribution of the proposed PCF sensor shows super-modes in the orientations of y-pol (a) ~ even mode, (b) ~ odd mode, and x-pol (c) ~ even mode and (d) ~ odd mode.

Table 1
Reference RI values of cancerous and normal cells for different human body organs.

Cancerous Cells	Medical Abbrevations	Refractive index of Cells		References
		Normal	Cancer	
CRT	HeLa	1.368	1.392	(Yasli, 2021; Jabin et al., 2019; Mishra et al., 2020)
BLD	Jurkat	1.376	1.395	(Yasli, 2021; Jabin et al., 2019; Mishra et al., 2020)
ADG	PC12	1.381	1.395	(Yasli, 2021; Jabin et al., 2019; Mishra et al., 2020)
BRT Type-1	MDA-MB-231	1.385	1.399	(Yasli, 2021; Jabin et al., 2019; Mishra et al., 2020)
BRT Type-2	MCF-7	1.387	1.401	(Yasli, 2021; Jabin et al., 2019; Mishra et al., 2020)

3. Result and discussions

3.1. Coupling length, birefringence and interference spectra

The proposed PCF sensor with a central hole allows for the detection of bio-analytes from healthy and cancerous cells in various human bodily organs. This detection is achieved by observing the effective refractive index difference (n_e - n_o) between the x-pol ~ even and ~ odd modes and the y-pol ~ even and ~ odd modes, which occurs upon the infiltration of bio-analytes into the core region of the PCF sensor. Fig. 4 (a) & (b) show that although the effective RI difference between the ~ x-pol and ~ y-pol modes is slightly different but their corresponding curve features are similar within the wavelength range of 1.4 μm to 2.0 μm. The ((n_e - n_o) of the proposed sensor has been observed to increase as the wavelength range increases, indicating a significant reduction in the coupling length (L_c), as shown in Fig. 4(c) & (d). Additionally, the PCF sensor exhibits birefringence as the E-field distribution of simulated supermodes reveals that even-distributed supermodes transmit more radiated energy into the penetrated center hole of the PCF than odd-

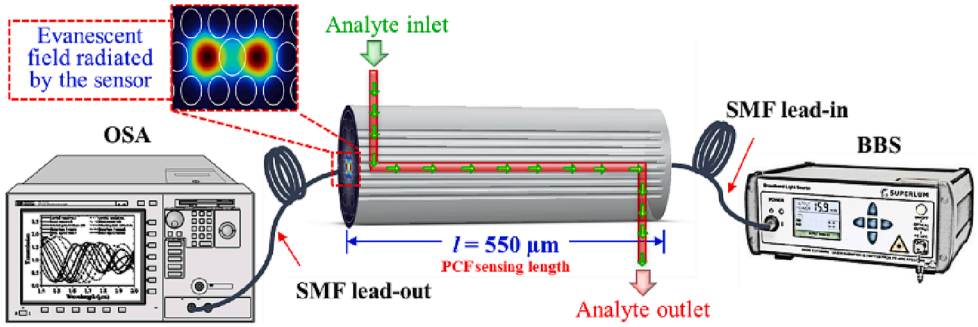

Fig. 3. A possible experimental setup for obtaining transmission spectra using the proposed PCF sensor.

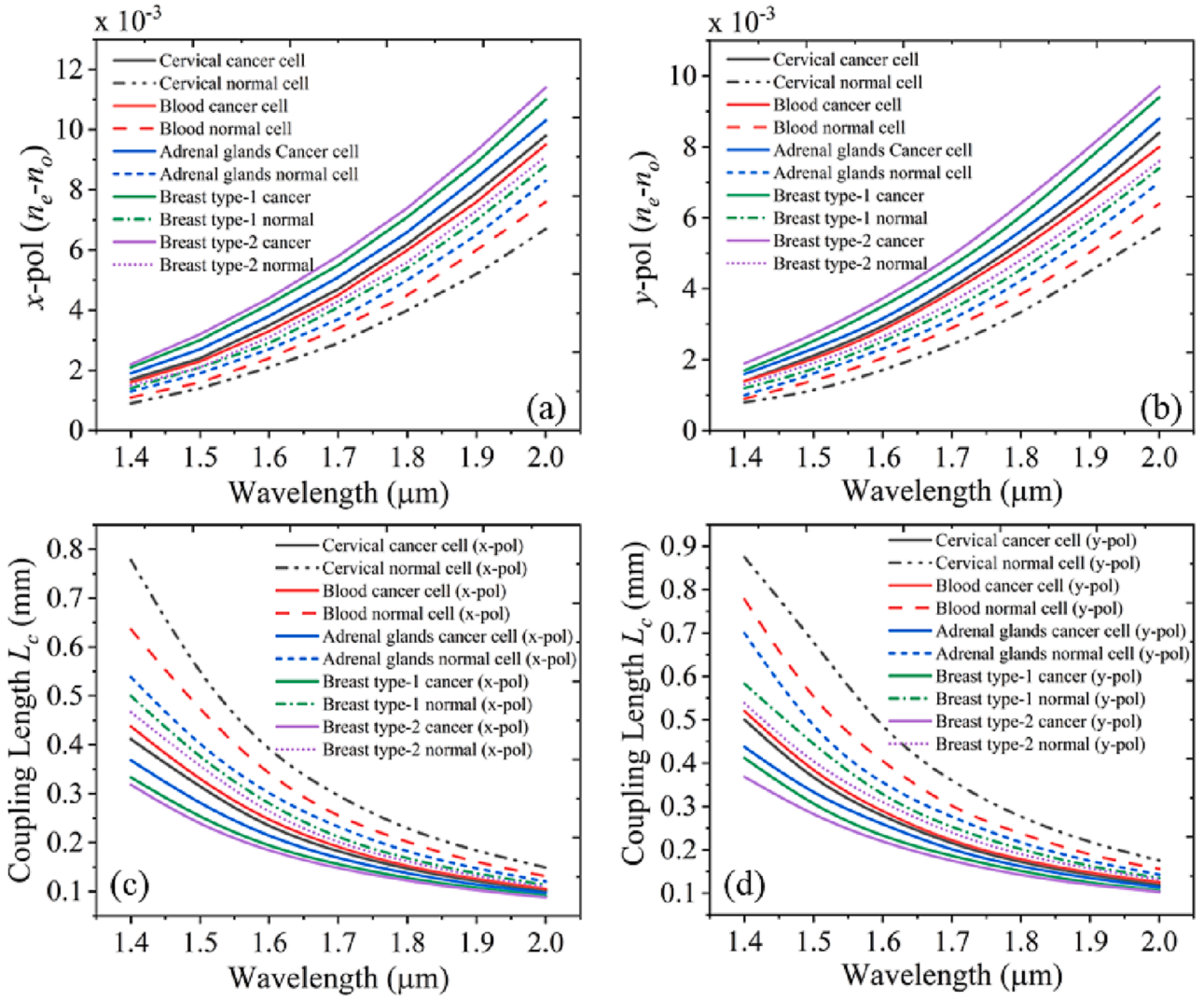

Fig. 4. Effective RI difference between even and odd (a) x-pol and (b) y-pol modes, as well as predicted PCF sensor coupling lengths for corresponding (c) x-pol and (d) y-pol modes.

distributed supermodes, as shown in Fig. 2. The L_c corresponding to the wavelength for the suggested structure can be calculated using coupled mode theory, as detailed in (Mishra et al., 2020).

$$L_c = \frac{\lambda}{2|n_e^i - n_o^i|}, \qquad i = x, y, \tag{2}$$

The birefringence in the proposed PCF sensor can be expressed as the difference between the effective refractive indices of the two orthogonal polarization modes that propagate in the PCF. Mathematically, the birefringence can be written as,

$$B(\lambda) = |n_{eff}^x - n_{eff}^y| \tag{3}$$

where n_{eff}^x is the effective refractive index for the polarization along the x-axis, and n_{eff}^y is the effective refractive index for the polarization along the y-axis. As depicted in Fig. 5, the birefringence of the PCF with varying analyte infiltration is determined. The results reveal an increase in birefringence towards the longer wavelength side, whereas a decrease is observed towards the shorter wavelength side. The birefringence of PCF is a valuable property with various benefits, including polarization control, optical sensing, non-linear optics, and high-performance fibers. In sensing applications, the birefringence in PCFs can significantly enhance the sensitivity and selectivity of optical sensors by differentiating between various analytes and achieving improved detection limits.

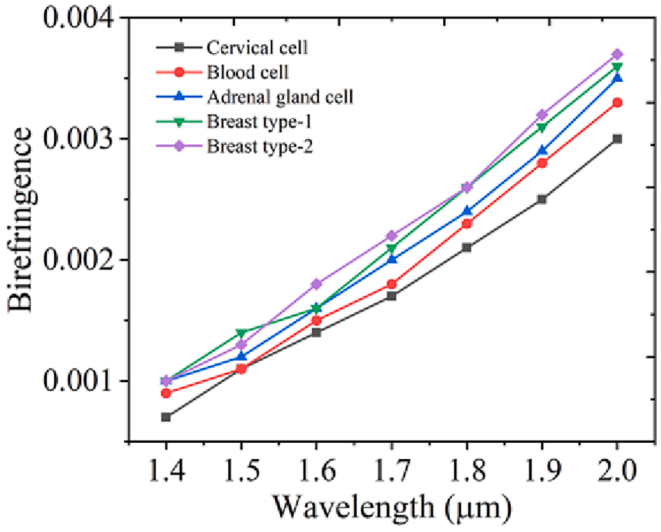

Fig. 5. Birefringence as a function of wavelength for different analytes.

The i-polarized even and odd distributed modes are represented by n_e^i and n_o^i, respectively. The transmission spectrum of the sensor is determined by the mode-coupling variations of the dual-core structure, which influences the transmission length based on the coupling length. The transmission optical power of the sensor proposed is calculated by (Biswas et al., 2018);

$$P_i(\lambda) = \sin^2\left(\frac{|n_e^i - n_o^i|\pi l}{\lambda}\right), \qquad i = x, y, \tag{4}$$

In order to reduce the sensing length for a miniaturized probe, the proposed sensor investigates through mode-coupling theory. To detect the carcinogenic MCF-7 analyte, the sensing length was adjusted to l = 300 μm, 550 μm, and 1000 μm, and the resulting transmission spectra were obtained. As shown in Fig. 6, the sensing length of 300 μm produced a single resonant dip with lower fringe visibility, while 550 μm resulted in two dips, and 1000 μm showed three dips. Based on these observations, a sensing length of 550 μm was selected, as it exhibited two resonant dips and one resonant peak that could track changes caused by bio-analytes. The optical power of the transmission spectrum varied between 0 to 2.

3.2. Sensitivity performance

To assess the performance of a sensor, sensitivity monitoring is essential. The sensitivity of a sensor can be determined by evaluating the wavelength shift in the interference transmission spectra corresponding to different analytes RI values, such as normal to malignant cancerous cells or vice versa (Mumtaz et al., 2022). The sensitivity of the proposed sensor can be estimated by (Sasi et al., 2021);

$$S(\lambda) = \frac{\Delta\lambda}{\Delta n} \quad (\text{nm/RIU}) \tag{5}$$

Fig. 7(a-e) depict the spectrum evolution of the proposed sensor when it is infiltrated with different types of normal and malignant cancerous cells of various human tissues, thereby enabling the monitoring of $\Delta\lambda$ and Δn. Here, Δn refers to the difference between the refractive indices of normal and malignant cancerous analytes, while $\Delta\lambda$ represents the displacement of the interference dip or peak in the transmission spectra. This information provides valuable insights into the performance of the sensor.

The proposed sensor was examined using cancerous and normal cells of various human body organs, such as CRT, BLD, ADG, and BRT cells, as depicted in Fig. 7(a-e). The transmission spectra showed the shift in dip and peak wavelengths as normal and malignant cancerous analytes progressed. The dip shift differences for resonant wavelengths between normal and malignant cancerous cells were measured as 190.56 nm, 115.71 nm, 136.46 nm, 126.09 nm, and 125.92 nm for CRT, BLD, ADG, BRT type-1, and type-2 cells, respectively, while the peak shift differences were measured as 209.87 nm, 150.19 nm, 122.09 nm, 141.57 nm, and 156.09 nm for correspondingly same category of cells. The detection limit ranged between 0.014 and 0.024 for the RIs of CRT, BLD, ADG, BRT type-1, and type-2 cells, respectively. Both malignant and normal CRT cells had the highest detection threshold. PCF Sensor exhibits optimal sensitivity of −7,940 nm/RIU, −8,265 nm/RIU, −9,747 nm/RIU, −9,006 nm/RIU, and −8,994 nm/RIU by peak shift and −8,745 nm/RIU, −10,728 nm/RIU, −8,721 nm/RIU, −10,113 nm/RIU, and −11,150 nm/RIU by dip shift for CRT, BLD, ADG, BRT type-1 and type-2 cells, respectively. The peak shift provided higher sensitivities than the dip shift. The maximum sensitivity for identifying breast type-2 cells was achieved using a wavelength peak shift of 11,150 nm/RIU, while the maximum sensitivity for detecting adrenal gland cells was −9,747 nm/RIU using a wavelength dip shift, as shown in Fig. 7(e) & 7(c), respectively. Additionally, the proposed sensor demonstrated a remarkable linear correlation function of R^2 = 0.99471 and R^2 = 0.98679 for wavelength dip and peak shift, respectively, with an average sensitivity of −8,708 nm/RIU and −9,293 nm/RIU in the RI range of 1.368 to 1.401, as shown in Fig. 7(f) encompassing normal and malignant cancerous cells such as CRT, BLD, ADG, BRT type-1, and type-2, which are further specified in Table 1.

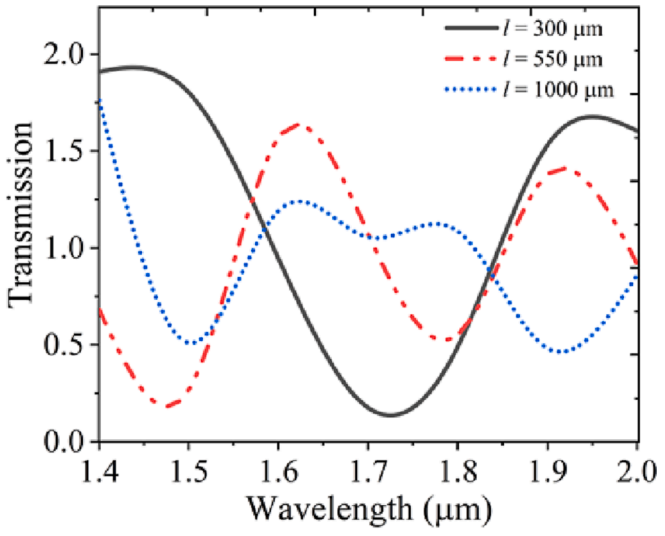

Fig. 6. The sensing length "l" is varied to acquire the transmission spectra (The core was filled with cancerous MCF-7 analyte).

3.3. Figure of merit

The proposed PCF sensor relies on detecting changes in the transmission spectra resulting from variations in the refractive index of analytes, making the Figure of Merit (FOM) a crucial parameter. The FOM for the proposed PCF sensor can be estimated as the sensitivity divided by the Full Width Half Maximum (FWHM), and mathematically can be written as,

$$\text{FOM} = \frac{S}{\text{FWHM}} \quad (\text{RIU}^{-1})$$

Sensitivity measures the sensor's output changes in response to an input stimulus, making it a useful metric to quantify the sensor's ability to detect small variations in the input. On the other hand, FWHM measures the width of the response curve at half its maximum amplitude, characterizing the resolution or bandwidth of a sensor's response. Fig. 8 indicates an impressive FOM range of 44 RIU-1 to 56 RIU-1 for the proposed PCF sensor, highlighting its high sensitivity to small changes in refractive index, which is calculated by dip and peak, respectively. This makes the sensor a suitable candidate for a wide range of applications, such as biological detection, environmental monitoring, and chemical sensing. However, it is important to remember that FOM is only one of many factors to consider when evaluating a sensor's performance.

The comparison of the proposed sensor with previously reported sensors provides valuable insights into its sensitivity and design advantages, as listed in Table 2. The proposed sensor demonstrates a dual sensing mechanism, which allows it to track both dip and peak shift simultaneously in the transmission spectra. This capability enhances its sensitivity and improves its ability to detect minute changes in the analyte RI. Additionally, the cladding region of the proposed sensor contains fewer air holes, which improves its waveguiding properties, further increasing its sensitivity.

Compared to previously reported sensors, the proposed sensor also boasts a simpler design, which makes it easier to manufacture. This advantage can significantly reduce the manufacturing costs, making the sensor more accessible and affordable to a wider range of applications. Moreover, the simpler design provides greater versatility in terms of the analytes to be detected, allowing it to be easily modified and customized for various target analytes.

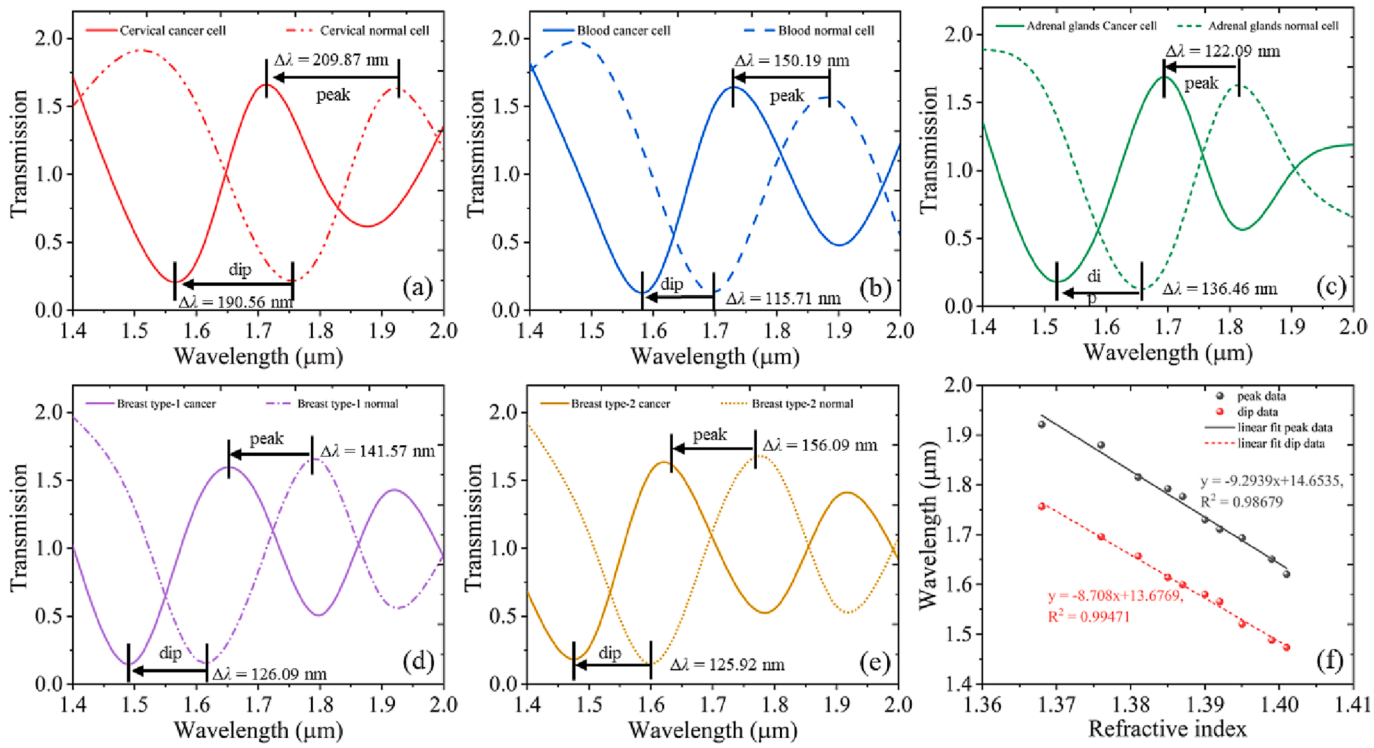

Fig. 7. Spectra evolution of the sensors when experiencing normal and cancerous cell analytes (a) CRT, (b) BRT, (c) ADG, (d) BRT type-1, (e) BRT type-2 cells, and (f) sensor's average sensitivity corresponding to dip and peak shift with linear correlation function.

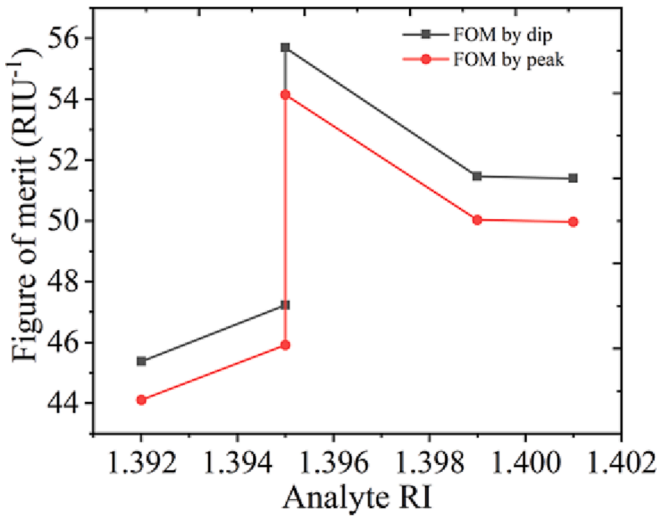

Fig. 8. Variation in Figure of Merit (FOM) values corresponding to cancerous cell analytes for the proposed PCF sensor.

3.4. Fabrication tolerance

Achieving optimal sensitivities depends significantly on the physical properties of the sensor, such as the diameter of the cladding air holes (d_a), the diameter of the center core hole (d_c), and the pitch distance (Λ) between the holes. To assess the effect of these properties on the sensor's performance, both normal and malignant cancerous cells (specifically MCF-7) were subjected to analysis for their RIs. The physical properties of the proposed sensor were evaluated based on the resonant peak shift, which exhibited superior sensitivity compared to dip shift.

As shown in Fig. 9(a), peak locations for MCF-7 normal cells are observed at 1641.31 nm, 1620.5 nm, and 1607.1 nm, whereas for malignant cancer cells, peaks are located at 1787.14 nm, 1776.6 nm, and 1743.5 nm, respectively, as d_a varies from 1.4 μm to 1.6 μm. The achieved sensitivities were −10,416 nm/RIU, −11,150 nm/RIU, and −9,742 nm/RIU, respectively, with fixed values of $d_c = 1.9$ μm and $\Lambda = 2.0$ μm. Optimal sensitivities were attained by modifying d_c and Λ. As shown in Fig. 9(b), the peak shift response for normal to malignant cancerous MCF-7 cell is presented. The best sensitivities of −9,331 nm/

Table 2
Peformance comparison of the proposed PCF sensor.

Ref.	Malignant cancerous cell	Spectral Sensitivity (nm/RIU) dip shift	peak shift	Detection threshold Δn
(Aly and Zaky, 2019)	CRT (Cervical)	2,166	–	0.024
	BLD (Blood)	2,175	–	0.014
	ADG (Adrenal gland)	2,156	–	0.014
	BRT type-1 (Breast)	2,163	–	0.014
	BRT typ-2 (Breast)	2,156	–	0.014
(Yasli, 2021)	CRT	4,333	–	0.024
	BLD	4,642	–	0.014
	ADG	5,500	–	0.014
	BRT type-1	6,428	–	0.014
	BRT typ-2	7,142	–	0.014
	Basal	3,150	–	0.014
(Mishra et al., 2020)	CRT (Cervical)	7,916	–	0.024
	BLD (Blood)	8,571	–	0.014
	ADG (Adrenal gland)	9,285	–	0.014
	BRT type-1 (Breast)	10,000	–	0.014
	BRT typ-2 (Breast)	10,000	–	0.014
This work	CRT (Cervical)	−7,940	−8,745	0.024
	BLD (Blood)	−8,265	−10,728	0.014
	ADG (Adrenal gland)	−9,747	−8,721	0.014
	BRT type-1 (Breast)	−9,006	−10,113	0.014
	BRT type-2 (Breast)	−8,994	−11,150	0.014

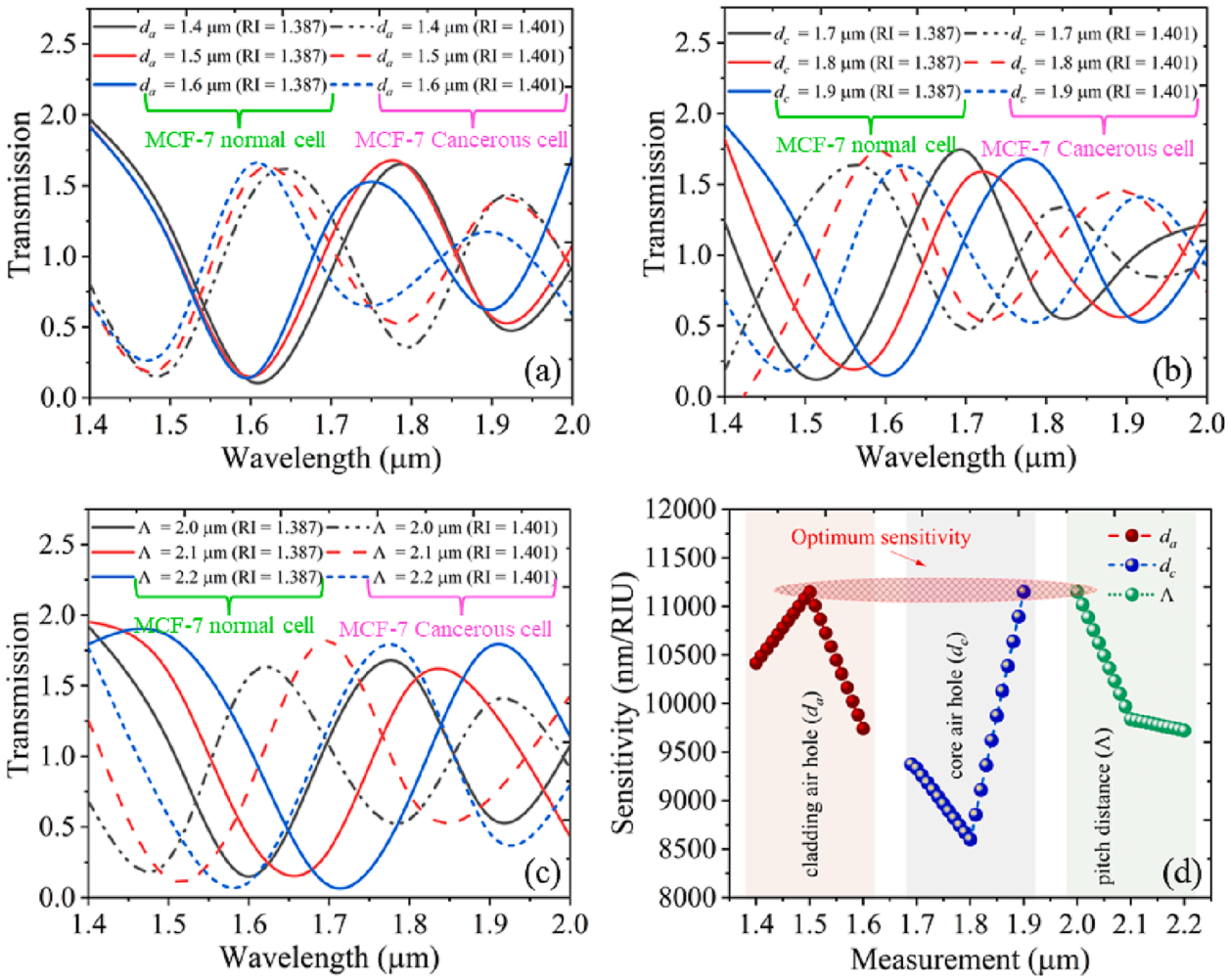

Fig. 9. Transmission Spectra is varied for (a) d_a (b) d_c, and (c) Λ; (d) Spectral sensitivity as a function of d_a, d_c, and Λ.

RIU, −8,600 nm/RIU, and −11,150 nm/RIU were obtained for corresponding d_c values ranging from 1.7 μm to 1.9 μm, while $d_a = 1.5$ μm and Λ = 2.0 μm were kept constant.

It was observed that the optimal sensitivity of −11,150 nm/RIU was achieved at Λ = 2.0 μm, as depicted in Fig. 9(c), upon varying the pitch distance (Λ) from 2.0 μm to 2.2 μm, however, $d_a = 1.5$ μm and $d_c = 1.9$ μm were kept constant. Table 3 provides a comprehensive view of the parametric variation associated with the achieved sensitivities, while Fig. 9(d) offers a graphical summary of the results obtained.

Table 3
Parameters involve in fabrication tolerance for the proposed PCF sensor.

Physical parameter	Peak position (λ)		Δλ (nm)	Δn	S (nm/RIU)
	Normal BRT type-2 (nm)	Cancerous BRT type-2 (nm)			
$d_a = 1.4$ μm	1787.14	1641.31	−145.83	0.014	−10,416
$d_a = 1.5$ μm	1776.61	1620.52	−156.09	0.014	−11,150
$d_a = 1.6$ μm	1743.5	1607.11	−136.39	0.014	−9,742
d_a is varied though $d_c = 1.9$ μm and Λ = 2.0 μm are fixed.					
$d_c = 1.7$ μm	1694.25	1563.61	−130.64	0.014	−9,331
$d_c = 1.8$ μm	1720.25	1599.86	−120.39	0.014	−8,600
$d_c = 1.9$ μm	1776.61	1620.52	−156.09	0.014	−11,150
d_c is varied though $d_a = 1.5$ μm and Λ = 2.0 μm are fixed.					
Λ = 2.0 μm	1776.61	1620.52	−156.09	0.014	−11,150
Λ = 2.1 μm	1834.06	1696.31	−137.75	0.014	−9,839
Λ = 2.2 μm	1911.22	1775.1	−136.12	0.014	−9,722
Λ is varied though $d_a = 1.5$ μm and $d_c = 1.9$ μm are fixed.					

3.5. Fabrication possibilities and advantages

Utilizing existing fabrication technologies, various methods are available for fabricating proposed microstructured PCF, however, each method has its own advantages and disadvantages. The stack and draw method (Pysz et al., 2014) involves stacking glass capillaries to form a preform, which is then heated and drawn to form the fiber. Although this method is straightforward, achieving high-quality structures is quite challenging. Sol-gel casting (Bise and Trevor, 2005) is a time-consuming and expensive process that involves using a solvent to form a preform from metal alkoxides. The preform method (Falkenstein et al., 2004) is then sintered to form the fiber, resulting in high-quality microstructured fibers. Prefrom drilling (Knight et al., 1997) is a widely used method where a preform is drilled with a laser to create the desired microstructure. This method can produce high-quality fibers, but it requires specialized equipment and skilled personnel. Extrusion (Ebendorff-Heidepriem et al., 2004) is a relatively simple and cost-effective method, but controlling the structure and dimensions of the fiber is difficult task. The outgassing of a porous preform (Guo et al., 2006) during draw involves creating a preform with a porous structure, which is then heated and drawn to form the microstructure. This method can produce high-quality fibers, but it is a complex and time-consuming process. Alternatively, the PCF can also be fabricated using the chemical vapor deposition (CVD) method (Knight et al., 1996), where a hollow silica tube is coated with layers of silica and dopants to achieve the desired refractive index profile. This method offers high flexibility in tailoring the refractive index profile and can produce large quantities of PCF with

uniform properties. However, it requires specialized equipment and may be more expensive compared to the other methods.

For the proposed PCF sensor, the best fit for fabrication would likely be the preform drilling method. This method allows for precise creation of the required microstructure with air holes in the cladding region using laser drilling. Additionally, this method has been shown to produce high-quality fibers and is widely used for fabricating microstructured fibers. However, the choice of fabrication method depends on various factors, including the desired structure, material, dimensions, and cost.

The proposed PCF-based optical sensor with dual demodulation offers several advantages for the early detection of critical malignant neoplastic cells in various human organs. The sensor has a high sensitivity, with optimal sensitivity values of −7,940 nm/RIU to −11,150 nm/RIU for peak and dip shift measurement, allowing for the detection of critical cancer cells at earlier stages. The use of a dual demodulation technique provides higher accuracy and selectivity. The sensor has a shorter sensing length of 550 μm, making it practical and easier to integrate into different systems. Furthermore, the birefringence property of PCF makes it a versatile tool for various applications such as polarization control, optical sensing, non-linear optics, and high-performance fibers. The early detection offered by the proposed sensor is particularly significant for cancer diagnosis and treatment, as it can improve patient outcomes by enabling early intervention. Overall, the proposed PCF-based optical sensor with dual demodulation is a promising tool for cancer diagnosis and treatment.

4. Conclusion

In conclusion, this study presents a promising approach for the detection of critical cancer cells in human organs using dual demodulation PCF structure. Through a numerical study, the proposed sensor demonstrated high sensitivity, provide fabrication feasibilities, and a straightforward approach for cancerous cells detection. The sensor design features a sunflower lattice-shaped dual-core PCF that facilitates optimal interaction between the E-field distribution and the specimen cells under test, resulting in accurate detection of malignant carcinogenic cells. The proposed PCF sensor achieved average sensitivities of −9,293 nm/RIU and −8,708 nm/RIU with peak and dip shift, respectively, for the detection of various cancerous cells in the RI range of 1.368 to 1.401, and showcasing excellent linearity of 0.996 and 0.997, respectively. The sensor also exhibited a birefringence by an order of 10^{-3}, indicating the ability to detect minute changes in refractive index. Additionally, the proposed sensor exhibited a high FOM in the range of 44 to 56 RIU^{-1}. These results make the proposed sensor an ideal candidate for biosensing applications, especially for early cancer detection phases. The high sensitivity and FOM, combined with the straightforward and easy fabrication process, suggest that the proposed sensor has the potential to become a valuable tool for clinicians and researchers alike. The results of this study are expected to pave the way for the development of more effective cancerous cells detection techniques that can ultimately contribute to improved patient outcomes and survival rates.

CRediT authorship contribution statement

Farhan Mumtaz: Conceptualization, Methodology, Software, Validation, Writing – original draft, Project administration.

Declaration of Competing Interest

The author declares that he has no known competing financial interests or personal relationships that could have appeared to influence the work reported in this paper.

Data availability

Data will be made available on request.

References

Abdelghaffar, M., Gamal, Y., Soliman, W., Badr, Y., Hameed, M.F.O., Obayya, S.S.A., 2022. Early cancer detection by plasmonic PCF sensor. In: Proceedings of the International Conference on Numerical Simulation of Optoelectronic Devices, NUSOD. 2022-Septe, pp. 147–148. doi: 10.1109/NUSOD54938.2022.9894779.

Ali, A.S., Ali, S., Ahmad, A., Bao, B., Philip, P.A., Sarkar, F.H., 2011. Expression of microRNAs: Potential molecular link between obesity, diabetes and cancer. Obesity Reviews. 12, 1050–1062. https://doi.org/10.1111/j.1467-789X.2011.00906.x.

Aly, A.H., Zaky, Z.A., 2019. Ultra-sensitive photonic crystal cancer cells sensor with a high-quality factor. Cryogenics (Guildf). 104, 102991 https://doi.org/10.1016/j.cryogenics.2019.102991.

Anders, B., Jesper, R., Stig, B.L., Jes, E.B., 2003. Photonic crystal fibres - novel fibres, new applications Anders. In: Proceedings of 2002 4th International Conference on Transparent Optical Networks (IEEE Cat. No.02EX551). IEEE, pp. 847–851 doi: 10.1038/nature01940.

Azzouz, A., Hejji, L., Kim, K.H., Kukkar, D., Souhail, B., Bhardwaj, N., Brown, R.J.C., Zhang, W., 2022. Advances in surface plasmon resonance–based biosensor technologies for cancer biomarker detection. Biosens Bioelectron. 197, 113767 https://doi.org/10.1016/j.bios.2021.113767.

Bekmurzayeva, A., Ashikbayeva, Z., Myrkhiyeva, Z., Nugmanova, A., Shaimerdenova, M., Ayupova, T., Tosi, D., 2021. Label-free fiber-optic spherical tip biosensor to enable picomolar-level detection of CD44 protein. Sci. Rep. 11, 1–13. https://doi.org/10.1038/s41598-021-99099-x.

Bise, R.T., Trevor, D.J., 2005. Sol-gel derived microstructured fiber: Fabrication and characterization. Conference on Optical Fiber Communication, Technical Digest Series 3, 269–271. https://doi.org/10.1109/ofc.2005.192772.

Biswas, S.K., Islam, S.M.R., Islam, M.R., Alam Mia, M.M., Sayem, S., Ahmed, F., 2018. Design of an ultrahigh birefringence photonic crystal fiber with large nonlinearity using all circular air holes for a fiber-optic transmission system. Photonics. 5, 26. https://doi.org/10.3390/photonics5030026.

Bulbul, A.A.M., Rahaman, H., Biswas, S., Hossain, M.B., A., 2020. Al Nahid, Design and numerical analysis of a PCF-based bio-sensor for breast cancer cell detection in the THz regime. Sens Biosensing Res. 30, 100388 https://doi.org/10.1016/j.sbsr.2020.100388.

Ebendorff-Heidepriem, H., Petropoulos, P., Asimakis, S., Finazzi, V., Moore, R.C., Frampton, K., Koizumi, F., Richardson, D.J., Monro, T.M., 2004. Bismuth glass holey fibers with high nonlinearity. Opt Express. 12, 5082–5087. https://doi.org/10.1364/opex.12.005082.

Eid, M.M.A., Rashed, A.N.Z., Bulbul, A.A.M., Podder, E., 2021. Mono-Rectangular Core Photonic Crystal Fiber (MRC-PCF) for Skin and Blood Cancer Detection. Plasmonics. 16, 717–727. https://doi.org/10.1007/s11468-020-01334-0.

Falkenstein, P., Merritt, C.D., Justus, B.L., 2004. Fused array preforms for the fabrication of photonic crystal fibers. Opt Lett. 29, 1858–1860. https://doi.org/10.1364/fio.2004.fwo3.

Guo, T., Lou, S., Fang, H., Jian, S., 2006. Research on the fabrication of photonic crystal fiber. Optoelectron Mater Devices. 6352, 738–745. https://doi.org/10.1117/12.688506.

Hecht, S.S., 2003. Tobacco carcinogens, their biomarkers and tobacco-induced cancer. Nat Rev Cancer. 3, 733–744. https://doi.org/10.1038/nrc1190.

Jabin, M.A., Ahmed, K., Rana, M.J., Paul, B.K., Islam, M., Vigneswaran, D., Uddin, M.S., 2019. Surface Plasmon Resonance Based Titanium Coated Biosensor for Cancer Cell Detection. IEEE Photonics J. 11, 1–10. https://doi.org/10.1109/JPHOT.2019.2924825.

N. Jamil, W.S. Khan, Detection of Cancer Cells by Using Biosensors, in: Nanobiosensors, Wiley, 2020: pp. 95–115. doi: 10.1002/9783527345137.ch5.

Kaur, B., Kumar, S., Kaushik, B.K., 2022. MXenes-based fiber-optic SPR sensor for colorectal cancer diagnosis. IEEE Sens J. 22, 6661–6668. https://doi.org/10.1109/JSEN.2022.3154385.

Knight, J.C., Birks, T.A., Atkin, D.M., Russell, P.S.J., 1996. Pure silica single-mode fibre with hexagonal photonic crystal cladding. Conf. Opt. Fiber Commun., Techn. Digest Series 339–342.

Knight, J.C., Birks, T.A., Russell, P.St.J., Atkin, D.M., 1997. All-silica single-mode optical fiber with photonic crystal cladding: errata. Opt Lett. 22, 484–485. https://doi.org/10.1364/ol.22.000484.

Loyez, M., Larrieu, J.C., Chevineau, S., Remmelink, M., Leduc, D., Bondue, B., Lambert, P., Devière, J., Wattiez, R., Caucheteur, C., 2019. In situ cancer diagnosis through online plasmonics. Biosens. Bioelectron. 131, 104–112. https://doi.org/10.1016/j.bios.2019.01.062.

Mishra, G.P., Kumar, D., Chaudhary, V.S., Murmu, G., 2020. Cancer cell detection by a heart-shaped dual-core photonic crystal fiber sensor. Appl Opt. 59, 10321–10329. https://doi.org/10.1364/ao.409221.

Mollah, M.A., Usha, R.J., Tasnim, S., Ahmed, K., 2020. Detection of cancer affected cell using Sagnac interferometer based photonic crystal fiber refractive index sensor. Opt Quantum Electron. 52, 1–12. https://doi.org/10.1007/s11082-020-02542-y.

Mollah, M.A., Yousufali, M., Ankan, I.M., Rahman, M.M., Sarker, H., Chakrabarti, K., 2020. Twin core photonic crystal fiber refractive index sensor for early detection of blood cancer. Sens Biosensing Res. 29, 100344 https://doi.org/10.1016/j.sbsr.2020.100344.

Mumtaz, F., Dai, Y., Ashraf, M.A., 2020. Inter-Cross De-Modulated Refractive Index and Temperature Sensor by an Etched Multi-Core Fiber of a MZI Structure. Journal of Lightwave Technology 38, 6948–6953. https://doi.org/10.1109/JLT.2020.3014857.

Mumtaz, F., Roman, M., Zhang, B., Abbas, L.G., Dai, Y., Ashraf, M.A., Fiaz, M.A., Kumar, A., 2022. MXene (Ti3C2Tx) coated highly-sensitive D-shaped photonic crystal fiber based SPR-biosensor. Photonics Nanostruct. 52, 101090 https://doi.org/10.1016/j.photonics.2022.101090.

Mumtaz, F., Roman, M., Zhang, B., Abbas, L.G., Ashraf, M.A., Fiaz, M.A., Dai, Y., Huang, J., 2022. A simple optical fiber SPR sensor with ultra-high sensitivity for dual-parameter measurement. IEEE Photon. J. 14, 1–7. https://doi.org/10.1109/JPHOT.2022.3203930.

Mumtaz, F., Yaseen, G., Roman, M., Lashari, G.A., Ashraf, M.A., Fiaz, M.A., Dai, Y., 2023. Numerical analysis of the highly non-linear and ultra-sensitive modified core of a photonic crystal fiber sensor for detection of liquid analytes. Journal of Optical Society of America B 40, 142–150. https://doi.org/10.1364/JOSAB.478468.

Mumtaz, F., Zhang, B., Roman, M., Ghulam, L., Aqueel, M., Dai, Y., 2023. Computational study : Windmill-shaped multi-channel SPR sensor for simultaneous detection of multi-analyte. Measurement 207, 112386. https://doi.org/10.1016/j.measurement.2022.112386.

Parvin, T., Ahmed, K., Alatwi, A.M., Rashed, A.N.Z., 2021. Differential optical absorption spectroscopy-based refractive index sensor for cancer cell detection. Opt Rev. 28, 134–143. https://doi.org/10.1007/s10043-021-00644-w.

Pysz, D., Kujawa, I., Stepien, R., Klimczak, M., Filipkowski, A., Franczyk, M., Kociszewski, L., Buzniak, J., Harasny, K., Buczynski, R., 2014. Stack and draw fabrication of soft glass microstructured fiber optics. Bull. Polish Acad Sci. Techn. Sci. 62, 667–682. https://doi.org/10.2478/bpasts-2014-0073.

Ramola, A., Marwaha, A., Singh, S., 2021. Design and investigation of a dedicated PCF SPR biosensor for CANCER exposure employing external sensing. Appl. Phys. A Mater. Sci. Process. 127, 1–20. https://doi.org/10.1007/s00339-021-04785-2.

Saha, A., Basak, P., Gupta, B., Sil, S., Pal, S., 2020. Radiated Cancer Cells : C band to THz perspective. In: 2020 IEEE International Conference on Electronics, ComputIng and Communication Technologies (CoNECCT), pp. 1–6. https://doi.org/10.1109/CONECCT50063.2020.9198520.

Samaras, V., Rafailidis, P.I., Mourtzoukou, E.G., Peppas, G., Falagas, M.E., 2010. Chronic bacterial and parasitic infections and cancer: A review. J. Infect. Dev. Ctries. 4, 267–281. https://doi.org/10.3855/jidc.819.

Sasi, S., Francis, S.M., Jacob, J., Thomas, V.I., 2021. A tunable plasmonic refractive index sensor with ultrabroad sensing range for cancer detection. Plasmonics. 16, 1705–1717. https://doi.org/10.1007/s11468-021-01418-5.

Schartner, E.P., Henderson, M.R., Purdey, M., Dhatrak, D., Monro, T.M., Gill, P.G., Callen, D.F., 2016. Cancer detection in human tissue samples using a fiber-tip pH probe. Cancer Res. 76, 6795–6801. https://doi.org/10.1158/0008-5472.CAN-16-1285.

Singh, R., Kumar, S., Liu, F.Z., Shuang, C., Zhang, B., Jha, R., Kaushik, B.K., 2020. Etched multicore fiber sensor using copper oxide and gold nanoparticles decorated graphene oxide structure for cancer cells detection. Biosens Bioelectron. 168, 112557 https://doi.org/10.1016/j.bios.2020.112557.

Sun, D., Ran, Y., Wang, G., 2017. Label-free detection of cancer biomarkers using an in-line taper fiber-optic interferometer and a fiber bragg grating. Sensors (Switzerland). 17, 2559. https://doi.org/10.3390/s17112559.

Taya, S.A., Sharma, A., Doghmosh, N., Colak, I., 2022. Detection of water concentration in ethanol solution using a ternary photonic crystal-based sensor. Mater Chem Phys. 279, 125772 https://doi.org/10.1016/j.matchemphys.2022.125772.

Yasli, A., 2021. Cancer Detection with Surface Plasmon Resonance-Based Photonic Crystal Fiber Biosensor. Plasmonics. 16, 1605–1612. https://doi.org/10.1007/s11468-021-01425-6.

Yoshikawa, Y., Emi, M., Nakano, T., Gaudino, G., 2020. Mesothelioma developing in carriers of inherited genetic mutations, Transl Lung. Cancer Res. 9, S67–S76. https://doi.org/10.21037/tlcr.2019.11.15.

Farhan Mumtaz (Member, IEEE) earned his Bachelor's degree in science from Punjab University Lahore, Pakistan, in 2006, his Master's degree in electronics from Quaid-i-Azam University Islamabad, Pakistan, in 2018, and his Ph.D. in information and communication engineering from Wuhan University of Technology, China, in 2021. From February 2022, he starts working in the Faculty of Electrical and Computer Engineering at Missouri University of Science and Technology, Rolla, MO, 65409-0040, USA where he is now serving as an Assistant Research Professor. From 2007 through 2015, he worked for Huawei Technologies (Pvt.) Ltd. in Islamabad, Pakistan, holding a number of important positions, including Plan Control Manager, Project Manager, and Service Solution Manager. His current research focuses on femtosecond laser micro-machining of optoelectronic materials, instrumentation of fiber optic sensors for energy and harsh environments for the US steelmaking industry, Silica and Sapphire based Fiber Bragg Gratings (FBGs), Rayleigh OFDR, Brillion OTDA/R, surface plasmons, biosensors, and photonic crystal fiber designs.